The Circumglobal North American wave pattern and its relation to North American cold events

Nili Harnik[1,2*], Gabriele Messori[2,3], Rodrigo Caballero[2,4], Steven B. Feldstein[5]

[1]Department of Geophysics and Planetary Sciences, Tel Aviv University, Tel Aviv, Israel
[2]Department of Meteorology, Stockholm University, Stockholm, Sweden
[3]Met Office Hadley Centre, Exeter, UK
[4]Bolin center for Climate Research, Stockholm University, Stockholm, Sweden
[5]Pennsylvania State University, PA, USA

Key Points:

- North American cold events are associated with the Circumglobal Teleconnection Pattern 2
- PNA events are related to Circumglobal Teleconnection Pattern 1 and are in quadrature with pattern 2
- The peak cold lags the upper level North American wave by 3 days, and an Asian wave by about 1 week

[*]Department of Geosciences, Tel Aviv University, Tel Aviv, Israel, currently on sabbatical at the Meteorology Department, Stockholm University

Corresponding author: Nili Harnik, harnik@tau.ac.il

Abstract

Extreme large scale North American cold events are associated with strong undulations in the tropospheric jet stream which bring cold polar air southward over the continent. Here we propose that these jet undulations are associated with the North American part of the Circumglobal Teleconnection Pattern - a pair of zonally oriented waves of zonal wavenumber 5 which are in zonal quadrature with each other. While the PNA is associated with the first circumglobal wave pattern, North American extreme cold events are associated with the second pattern. The $300-hPa$ meridional wind and surface temperature anomalies associated with the Circumglobal North American wave packet are similar to those associated with the strongest Eastern US cold events. Both types of events are associated with a wave packet propagating all the way from Asia over the Pacific and across North America, with anomalous cold temperatures spreading south-eastwards from Canada over the continent.

1 Introduction

The tropospheric polar vortex has gained unprecedented media attention during the past few winters, when large undulations in the jet stream formed over North America along with extreme winter conditions. This was most notable during the winter of 2013-14 [e.g *Wallace et al.*, 2014; *Baxter and Nigam*, 2015; *Davies*, 2015; *Lee et al.*, 2015; *Yu and Zhang*, 2015; *Waugh et al.*, 2016; *Watson et al.*, 2016], but also during winter 2014-15 and February 2016[1]). The occurrence of such severe cold events during recent years which are globally amongst the warmest on record points to the differences between regional and global climate change; specifically, it highlights the need to fully understand the physical drivers or the events and their representation in climate models in order to robustly predict possible future changes in their frequency and intensity.

The dynamical drivers of cold events over North America have been studied extensively, using a diverse range of definitions for the cold events themselves [e.g. *Konrad*, 1996; *Walsh et al.*, 2001; *Portis et al.*, 2006; *Loikith and Broccoli*, 2012; *Grotjahn et al.*, 2015; *Messori et al.*, 2016, and references therein]. A robust finding of these studies is the association of North American cold events with large scale circulation anomalies which advect very cold air equatorward, typically from the northwest. A common finding is also that these large scale circulation anomalies are similar in scale and structure to the Pacific/North American (PNA) pattern, but the two patterns are zonally shifted, and thus project weakly onto each other [e.g. *Walsh et al.* [2001]; *Cellitti et al.* [2006]; *Grotjahn et al.* [2015]; *Messori et al.* [2016] also *Davies, 2015*, for winter 2013-14]. On the other hand, *Linkin and Nigam* [2008] noted a relation between North American cold air outbreaks and the North Pacific Oscillation [NPO, *Walker and Bliss*, 1932] and its associated upper level West Pacific (WP) teleconnection pattern.

Here we propose that the large scale circulation anomalies which drive cold events over North America east of the Rockies are associated with the Circumglobal Teleconnection Pattern (CTP) introduced by *Branstator* [2002]. *Branstator* [2002] obtained the CTP from the first two EOFs of monthly mean seasonal anomalies of Dec-Feb $300-hPa$ nondivergent meridional wind. The two patterns together represent a zonally oriented medium scale wave train of zonal wave 5 with arbitrary zonal phasing. *Feldstein and Dayan* [2008] showed that on daily time scales, these patterns appear as localized wave packets which propagate downstream with an eastward group speed and near zero phase speed [see also *Watanabe*, 2004; *Yuan et al.*, 2011]. These yield a circumglobal wave pattern when averaged over time [*Feldstein and Dayan*, 2008].

The zonal scale of the CTP is similar to the jet stream undulations as seen in the 2013-14 winter (the longitudinal span of the North American landmass is roughly zonal wavenumber 5), and we may expect its quasi-stationary nature to allow for persistent advection of cold

[1] See $http://www.cpc.ncep.noaa.gov/products/CDB/CDB\_Archive\_html/CDB\_archive.shtml$

polar air across the continent. It is therefore plausible that the CTP may play a role in driving North American extreme cold events. The CTP has been associated with extreme weather during summer [*Schubert et al.*, 2011; *Teng et al.*, 2013], and with winter precipitation over Israel [*Feldstein and Dayan*, 2008], but has not been studied in the context of North American winter weather. Recently, *Messori et al.* [2016] composited extreme Eastern US cold events, and showed a zonally oriented wave pattern with a wavelength corresponding roughly to zonal wave number 5 and a phasing similar to the second CTP pattern, which propagates from the Pacific over North America to the Atlantic (see their Figure 2). In this paper, we explicitly examine the relation of this wave pattern to the second CTP, by comparing surface temperature and upper level flow fields during times when the flow projects strongly onto the North American part of the CTP, and during extreme cold events over the eastern US. The linking of the two phenomena has possible implications for predictability [*Teng et al.*, 2013; *Grazzini and Vitart*, 2015], which we will briefly explore by examining the upstream origins and precursors of the North American part of the CTP.

2 Data and analysis methods

We use daily anomalies, defined by removing a smoothed daily climatology (using a 21 day running mean). The events are calculated using daily mean and monthly mean gridded fields from ERA-Interim [*Dee et al.*, 2011] for 1979-2014. Much of the analysis for the CTP based events was repeated using NCEP I reanalysis [*Kalnay et al.*, 1996] from 1958-2015 and except where noted, the results are similar.

The statistical significance of the composites is calculated both using a 500 member boot strap method and a sign-test which indicates where a certain percentage of composite members have the same sign as the composite mean. The chances for a given percentage of events to have the same sign as the composite mean is determined using a binomial formula, assuming equal chances for positive and negative anomalies. Spatial correlations between two patterns are calculated after weighting each by square root of cosine latitude, and the statistical significance is estimated by correlating one of the patterns with the corresponding field from 1000 randomly chosen days. We define several kinds of events, as follows:

2.1 The Circumglobal North American (CNA) wave pattern

To obtain a regional CTP index, we begin by calculating the global CTP patterns using a method similar to *Branstator* [2002]. The global CTPs are the first two EOFs of the winter anomalies of monthly mean $300-hPa$ meridional wind, calculated by removing each season's Dec-Feb mean fields from the monthly mean meridional wind fields. A square root of cosine latitude weighting is used for the analysis (so that the variance is weighted by a cosine latitude). Unlike *Branstator* [2002], we use the full meridional wind, rather than non divergent meridional wind, since the two give very similar results. We note that without removing the seasonal mean anomalies, the first EOF has a planetary scale, and using daily fields gives a pair of zonal wavenumber 6 patterns for the first EOFs .

Using monthly ERA-Interim data, the first two EOFs (shading, Figure 1) are a pair of quasi zonal wave number 5 patterns which explain 13.3 and 11.5 percent of the variance, and are not well separated according to the *North et al.* [1982] criterion, suggesting that they span a continuum of zonal wave number 5 patterns with arbitrary phase. The robustness of these patterns is examined using NCEP and discussed in the supplementary information (Figure S1). Following *Feldstein and Dayan* [2008], we obtain daily regional CTP indices by projecting the daily $300-hPa$ meridional wind anomalies onto specific zonal sectors of the global CTPs (see supplementary information for details). For the North American region, we choose the domain $180-324^oE$, $10-85^oN$ (see the boxes in Figure 2c,d), where the longitudinal span of 144^o was chosen to capture two full wavelengths of zonal wave 5. We then project the daily data onto the second CTP pattern in this region. We refer to this pattern as the Circumglobal North American (CNA) pattern, and to its normalized projection as the CNA index.

To define positive CNA events, we find the days on which the 5-day running mean of the CNA index exceeds its mean by one standard deviation. We define the peak value to be the event center, with events being separated by at least one day in which the index drops below one half a standard deviation above the mean. We find 78 positive events for ERA-Interim (and 123 events for NCEP). We do not impose any additional time separation, but find that the vast majority of events are separated by 7 or more days.

2.2 The Circumglobal Eurasian wave pattern

To examine the possibility of precursor patterns, we repeat the procedure done for CNA events, using a Eurasian region: $0-144^oE$, $10-85^oN$ (see the box in Figure 4a), and define events in a similar manner. We find 79 events using ERA-Interim and 139 events in NCEP.

2.3 Eastern United States Cold (USC) events

We rank Eastern United States Cold (USC) events based on the area weighted 2-meter temperature anomaly over the region $100-70^oW$, $30-45^oN$ (see box in Figure 2f). This is the same region used by *Messori et al.* [2016]. The normalized area-weighted temperature time series is referred to as the USC index. To choose USC events we smooth the temperature anomalies using a 5-day running mean, and choose the days with the largest negative temperature anomaly. We discard events which are closer than 7 days to another event, keeping the colder event of the two. For comparison with the CNA event composites, we choose the 78 coldest events, which consist of an area-weighted anomaly below $-4.7K$.

2.4 Daily Pacific North American (PNA) pattern

We calculate a daily Pacific North American (PNA) index by combining the standardised 500 hPa geopotential height anomalies at (20N, 160W), (45N, 165W), (55N, 115W) and (30N, 85W), following *Wallace and Gutzler* [1981] and *Cellitti et al.* [2006], and normalizing the resulting index to have unit standard deviation. Positive events are defined by the index exceeding 1.0.

3 Results

Figure 1 shows the first two CTP patterns of anomalous $300-hPa$ meridional wind, along with the anomalous $300-hPa$ meridional wind composites for day 0 positive PNA events and day -3 USC events. We note that the first CTP in its positive phase corresponds to anomalous poleward flow over Alaska, with anomalous equatorward flow on its sides. This pattern fits the positive phase of the PNA (compare the shading and contours in the left panel). The meridional wind anomaly associated with the coldest 78 USC events, on the other hand is in phase with the second CTP pattern (compare shading and contours in the right panel). This motivates us to further examine the relation between USC events and times when the flow projects strongly onto the second CTP over North America (which we have defined as CNA events). Before doing so, we note that the two CTPs are roughly in quadrature over the Pacific-North American region. Since the PNA projects strongly onto the first CTP while USC events project onto the second CTP, we expect the simultaneous correlation between the PNA and USC indices to be weak [as was found by *Cellitti et al.*, 2006; *Grotjahn et al.*, 2015; *Messori et al.*, 2016]. Indeed, the correlation between the PNA and USC indices reaches only -0.26 (at lag 0), compared to a correlation of 0.73 between the PNA and an index similar to the CNA but based on the first, rather than the second CTP.

Figure 2 shows the time lagged composites of $300-hPa$ meridional wind anomaly overlain on the full CTP EOF2, for CNA and USC events. The black boxes show the projection region used for defining the CNA events. The highest spatial correlation between the CNA and USC composites, with a value of 0.86 (statistically significant above the 99.9% level), is found

when USC events lag the CNA events by 3 days, thus we show the composites with a 3 day offset. We see a very clear similarity between the meridional wind pattern for both types of events. The patterns show a localized wavy pattern, with the wave packet amplitude propagating in time from Asia, over the Pacific and onto North America, but individual positive and negative centers being quasi-stationary. In both cases, we see a precursor wave packet over Asia with a clear branch along the subtropical jet and another more northward branch. The wave packets span roughly 3 full wavelengths at CNA day 0, their amplitude peaks shift eastward with a group speed of about 20^o longitude per day corresponding to about one week to travel from the Western Pacific to the Atlantic, and they have an almost zero eastward phase speed. This yields an equatorward flow over the northeastern North American continent, which is strong and significant for more than one week, making these quasi-stationary wave packets efficient in driving temperature anomalies.

Figure 3 shows the surface temperature composites for both kinds of events (right and left columns), with the USC fields shifted 3 days earlier than the CNA events. We see a strong similarity between the two types of events with the peak cold anomaly covering most of North America and a warm anomaly over Alaska and the Bering sea, at USC lag 0, CNA lag 3. At these times, both anomalies reach their coldest values over North America, and the spatial correlation between the two fields is maximal (0.85, statistically significant above the 99.9% level). The time evolution is also quite similar, with the peak USC cold anomaly starting from the northwest, spreading over most of the continent and shifting towards the east coast. The CNA cold anomalies do not shift meridionally in time as much as the USC events, and they are preceded by stronger anomalies over the Pacific Ocean and over Asia at early time lags, suggesting the Asian wave packet precursor temperature signal is more robust for CNA events. We note that the NCEP 2-meter temperature, which is derived differently from ERA Interim, shows slightly weaker and shorter lasting cold anomalies for the CNA events (Figure S2), and the ocean 2-meter temperature anomalies are absent.

Also shown (middle column) is the number of CNA composite members which have the same sign as the composite mean at each grid point (the *hit-rate*). Much of the statistically significant cold anomalies occur in more than 65% of the CNA events, and at the peak cold anomaly, in more than 75% and even 85% of the events (the chances of this happening randomly are much less that 1%). Of the 76 CNA events (we exclude two because at lag -7 they overlap with the peak of the preceding event), 30 are followed within 7 days by one of the 78 coldest spells identified here, exceeding the 95% statistical significance level obtained from random sampling. It is found that 44 of the events are followed by a cold event with temperatures below the 5th percentile of the full wintertime distribution, again above the 95% statistical significance level. The time correlation between the daily Dec-Feb (DJF) USC and CNA indices peaks when the US cold conditions lag the CNA pattern by 3 days, and is -0.45 (statistically significant at the 99.99% level, assuming a conservative 3 degrees of freedom per winter). We further find that 36.9% of the days on which the USC index is less than -1.0 are preceded 3 days earlier by a CNA index above 1.0 standard deviation, and 62% are preceded by a CNA projection above 0.5 standard deviations (see the conditional CNA distribution for all days vs strongly negative USC days in Figure S3). During the 2013-14 winter there was a succession of periods with a strong positive projection onto the CNA pattern, followed by extreme cold anomalies and negative USC values (Figure S4). Explicitly, the DJF mean normalised USC index was -0.6 with 37 days (41%) with a USC index below -1.0 standard deviation, compared to 5.9% of all 1980-2014 winter (DJF) days. The DJF mean normalised CNA index was 0.74 with 32 days (36%) with a CNA index larger than 1.0 standard deviation, compared to 5.3% of all 1980-2014 winter days.

The precursor Asian wave packet found in Figure 2 suggests a predictability pathway on a 7-10 day time scale for eastern North American cold events. To check this further we examine composites based on Eurasian CTP2 events, defined by the black rectangular region marked in the top left panel of Figure 4. We see a clear Eurasian wave packet at day zero, with corresponding statistically significant temperature anomalies being cold over the Middle East and

Siberia, and warm over Central Asia (not shown). There is a clear downstream group propagation over the Pacific and onto North America, leading to persistent and significant northerly flow anomalies over eastern North America, in phase with CTP2. Consistently, after lag 7 we see a gradual development of significant cold anomalies over the eastern US, reaching a peak around day 11, in some regions occurring in more than 67% of composite members (these anomalies are also found in NCEP though in a smaller more poleward region, Figure S5). We further count how many Eurasian wave packet events were followed by one of the 78 coldest USC events, 8-12 days later. This choice of range of lags is made to in order to include both day 9, when the spatial correlation with the corresponding surface temperature anomalies over the CNA area is highest (0.7, statistically significant at the 99% level), and day 11, when the strongest temperature anomalies (Figure 4f) take place. We find this happens for 9 of the 77 Eurasian wave packets (excluding two which overlap at lag $+11$ of the peak of the preceding event), which is exactly the 90th percent statistical significance level.

4 Discussion

We have shown that a large number of the extreme North American cold events have been driven by jet stream undulations similar to the CNA pattern. The statistical link between the CNA and North American cold events is significant and robust, though not all days with a strong projection onto the CNA lead to an extreme USC event a few days later, and not all extreme USC events are preceded by a strong projection onto the CNA. It does point, however, to a potential predictability pathway on 7-10 days, resulting from downstream propagation of the waves from Asia, and identifies potential precursor patterns. *Grazzini and Vitart* [2015] used an objective wave packet tracking algorithm and a forecast verification database and found increased predictability for long lasting wave packets originating in the West Pacific. They did not differentiate, however, between synoptic scale propagating waves and medium scale quasi stationary waves like the CTP, but it is very probable that these different types of wave packets affect predictability differently.

Bao and Wallace [2015] recently performed a cluster analysis of Northern Hemisphere 10 day low pass filtered $500\ hPa$ geopotential heights. They found four reproducible patterns, three of which they related to the NAO and PNA phases. Their second pattern, which was suggestive of Alaska blocking with a downstream wave train extension over North America, is similar to the positive CNA pattern. More examination is required to establish this connection robustly, but it suggests that the CNA may be a dominant recurring pattern of variability of the Northern Hemisphere wintertime flow.

An explicit examination of the 2013-14 winter shows that the projection onto the positive phase of the CNA was strong during many of the days that winter, suggesting that the cold events were associated with this flow pattern. This is consistent with *Wang et al.* [2014] and *Davies* [2015] who also noted a wave train propagating from the Pacific, resulting in a strong trough-ridge anomaly over the Gulf of Alaska-Great Lakes. *Linkin and Nigam* [2008] related the NPO/WP pattern to North American cold air outbreaks, and *Baxter and Nigam* [2015] and *Yu and Zhang* [2015] associated it with the winter of 2013-14. A comparison of the NPO/WP pattern [see e.g. Figure 3a of *Linkin and Nigam*, 2008] with the CNA suggests that they project strongly onto each other in some regions but the two are not the same.

A few recent studies of the extreme North American winter of 2013-14 have suggested that the anomalous ridge-trough pattern was forced by the anomalous Pacific SST anomalies during that winter [*Wang et al.*, 2014; *Baxter and Nigam*, 2015; *Hartmann*, 2015; *Lee et al.*, 2015; *Seager et al.*, 2015; *Yu and Zhang*, 2015; *Watson et al.*, 2016]. *Watson et al.* [2016] further obtained an improved forecast of the anomalous circulation over North America when the tropics were relaxed to ERA Interim observations, suggesting the forcing of divergent flow by SST anomalies [e.g. via excitation of Rossby wave sources *Sardeshmukh and Hoskins*, 1988] plays a central role. This raises the possibility that the CNA is excited or enhanced by SST

anomalies and points to the need for a better understanding of CNA drivers and of its possible interactions with SSTs and climate change.

Acknowledgments

The work was supported by the Israeli Science Foundation grant number 1537/12. The work was done when NH was on sabbatical at Stockholm University, supported by a Rossby Visiting Fellowship from the International Meteorological Institute of Stockholm University. SBF was supported by National Science Foundation grant AGS-1401220. Many of calculations presented here were performed using GOAT (Geophysical Observation Analysis Tool), a freely available MATLAB based tool for retrieval, analysis and visualisation of geophysical data (http://www.goat-geo.org). ECMWF ERA-Interim data used in this study have been obtained from the ECMWF Data Server http://data-portal.ecmwf.int/data/d/interim_daily/.

References

Bao, M., and J. M. Wallace (2015), Cluster analysis of northern hemisphere wintertime 500-hpa flow regimes during 1920–2014, *Journal of the Atmospheric Sciences*, *72*, 3597–3608.

Baxter, S., and S. Nigam (2015), Key role of the north pacific oscillation–west pacific pattern in generating the extreme 2013/14 north american winter, *Journal of Climate*, *28*(20), 8109–8117.

Branstator, G. (2002), Circumglobal teleconnections, the jet stream waveguide, and the north atlantic oscillation, *J. Clim.*, *15*, 1893–1910.

Cellitti, M. P., J. E. Walsh, R. M. Rauber, and D. H. Portis (2006), Extreme cold air outbreaks over the united states, the polar vortex, and the large-scale circulation, *JGR*, *111*(doi:10.1029/2005JD006273).

Davies, H. C. (2015), Weather chains during the 2013/2014 winter and their significance for seasonal prediction, *Nature Geoscience*, *DOI: 10.1038/NGEO2561*.

Dee, D. P., et al. (2011), The ERA-Interim reanalysis: configuration and performance of the data assimilation system., *Q. J. R. Meteorol. Soc.*, *137*, 553–597, 10.1002/qj.828.

Feldstein, S. B., and U. Dayan (2008), Circumglobal teleconnections and wave packets associated with israeli winter precipitation, *Quarterly Journal of the Royal Meteorological Society*, *134*(631), 455–467, doi:10.1002/qj.225.

Grazzini, F., and F. Vitart (2015), Atmospheric predictability and rossby wave packets, *Quarterly Journal of the Royal Meteorological Society*, *141*(692), 2793–2802, doi:10.1002/qj.2564.

Grotjahn, R., R. Black, R. Leung, M. F. Wehner, M. Barlow, M. Bosilovich, A. Gershunov, W. J. Gutowski, J. R. Gyakum, R. W. Katz, Y.-Y. Lee, Y.-K. Lim, and Prabhat (2015), North american extreme temperature events and related large scale meteorological patterns: a review of statistical methods, dynamics, modeling, and trends, *Climate Dynamics*, *46*(3), 1151–1184, doi:10.1007/s00382-015-2638-6.

Hartmann, D. L. (2015), Pacific sea surface temperature and the winter of 2014, *Geophysical Research Letters*, *42*(6), 1894–1902, doi:10.1002/2015GL063083, 2015GL063083.

Kalnay, E., et al. (1996), The NCEP/NCAR 40-year reanalysis project, *B. Am. Meteorol. Soc.*, *77*(434-471).

Konrad, C. E. I. (1996), Relationships between the intensity of cold air outbreaks and the evolution of synoptic and planetary scale features over north america, *MWR*, *124*, 1067–1083.

Lee, M.-Y., C.-C. Hong, and H.-H. Hsu (2015), Compounding effects of warm sea surface temperature and reduced sea ice on the extreme circulation over the extratropical north pacific and north america during the 2013–2014 boreal winter, *Geophysical Research Letters*, *42*(5), 1612–1618, doi:10.1002/2014GL062956, 2014GL062956.

Linkin, M. E., and S. Nigam (2008), The north pacific oscillation–west pacific teleconnection pattern: Mature-phase structure and winter impacts, *Journal of Climate*, *21*(9), 1979–1997.

Loikith, P. C., and A. J. Broccoli (2012), Characteristics of observed atmospheric circulation patterns associated with temperature extremes over north america, *Journal of Climate*, *25*(20), 7266–7281, doi:10.1175/JCLI-D-11-00709.1.

Messori, G., R. Caballero, and M. Gaetani (2016), On cold spells in north america and storminess in western europe, *GRL*, *43*, 6620–6628, doi:DOI: 10.1002/2016GL069392.

North, G. R., T. L. Bell, R. F. Cahalan, and F. J. Moeng (1982), Sampling errors in the estimation of empirical orthogonal functions, *Monthly Weather Review*, *110*(7), 699–706.

Portis, D. H., M. P. Cellitti, W. L. Chapman, and J. E. Walsh (2006), Low-frequency variability and evolution of north american cold air outbreaks, *Monthly Weather Review*, *134*(2), 579–597, doi:10.1175/MWR3083.1.

Sardeshmukh, P. D., and B. J. Hoskins (1988), The generation of global rotational flow by steady idealized tropical divergence, *J. Atmos. Sci.*, *45*(7), 1228–1251.

Schubert, S., H. Wang, and M. Suarez (2011), Warm season subseasonal variability and climate extremes in the northern hemisphere: The role of stationary rossby waves, *Journal of Climate*, *24*(18), 4773–4792, doi:10.1175/JCLI-D-10-05035.1.

Seager, R., M. Hoerling, S. Schubert, H. Wang, B. Lyon, A. Kumar, J. Nakamura, and N. Henderson (2015), Causes of the 2011–14 california drought, *Journal of Climate*, *28*(18), 6997–7024.

Teng, H., G. Branstator, H. Wang, G. A. Meehl, and W. M. Washington (2013), Probability of us heat waves affected by a subseasonal planetary wave pattern, *Nature Geosci*, *6*(12), 1056–1061.

Walker, G. T., and E. W. Bliss (1932), World weather v, *Memoires of the Royal Meteorological society*, *4*(36), 53–84.

Wallace, J. M., and D. S. Gutzler (1981), Teleconnections in the geopotential height field during the Northern Hemisphere winter, *Mon. Wea. Rev.*, *109*, 784–812.

Wallace, J. M., I. M. Held, D. W. Thompson, K. E. Trenberth, and J. E. Walsh (2014), Global warming and winter weather, *Science*, *343*(6172), 729–730.

Walsh, J. E., A. S. Phillips, D. H. Portis, and W. L. Chapman (2001), Extreme cold outbreaks in the united states and europe, 1948-99, *Journal of Climate*, *14*, 2642–2658.

Wang, S.-Y., L. Hipps, R. R. Gillies, and J.-H. Yoon (2014), Probable causes of the abnormal ridge accompanying the 2013–2014 california drought: Enso precursor and anthropogenic warming footprint, *Geophysical Research Letters*, *41*(9), 3220–3226, doi:10.1002/2014GL059748, 2014GL059748.

Watanabe, M. (2004), Asian jet waveguide and a downstream extension of the north atlantic oscillation, *Journal of Climate*, *17*(24), 4674–4691, doi:10.1175/JCLI-3228.1.

Watson, P. A. G., A. Weisheimer, J. R. Knight, and T. N. Palmer (2016), The role of the tropical west pacific in the extreme northern hemisphere winter of 2013/2014, *Journal of Geophysical Research: Atmospheres*, *121*(4), 1698–1714, doi:10.1002/2015JD024048, 2015JD024048.

Waugh, D. W., A. H. Sobel, and L. M. Polvani (2016), What is the polar vortex and how does it influence weather?, *BAMS*, *in press*, doi:doi:10.1175/BAMS-D-15-00212.1.

Yu, B., and X. Zhang (2015), A physical analysis of the severe 2013/2014 cold winter in north america, *Journal of Geophysical Research: Atmospheres*, *120*(19), 10,149–10,165, doi:10.1002/2015JD023116, 2015JD023116.

Yuan, J., S. B. Feldstein, S. Lee, and B. Tan (2011), The relationship between the north atlantic jet and tropical convection over the indian and western pacific oceans, *J. Clim.*, *24*, 6100–6113.

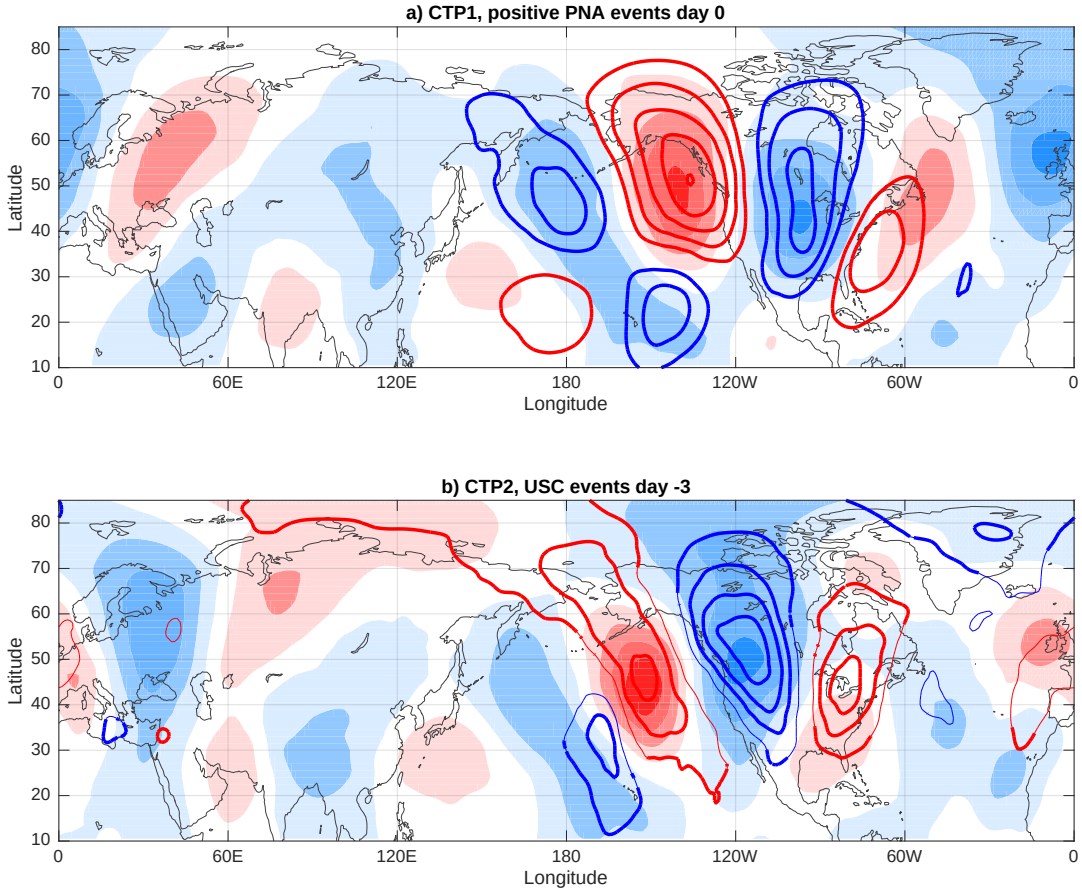

Figure 1. a) The first EOF of monthly mean seasonal anomalies of $300 - hPa$ meridional winds (shading) and the meridional wind composite of positive PNA events (red-blue contours) using Dec-Feb data. b) The second EOF of monthly mean seasonal anomalies of $300 - hPa$ meridional winds (shading) and the meridional wind composite of Eastern US Cold events (78 coldest events, red-blue contours). Contour interval is 3m/sec, red is positive and blue negative, thick lines are statistically significant at the 95% level.

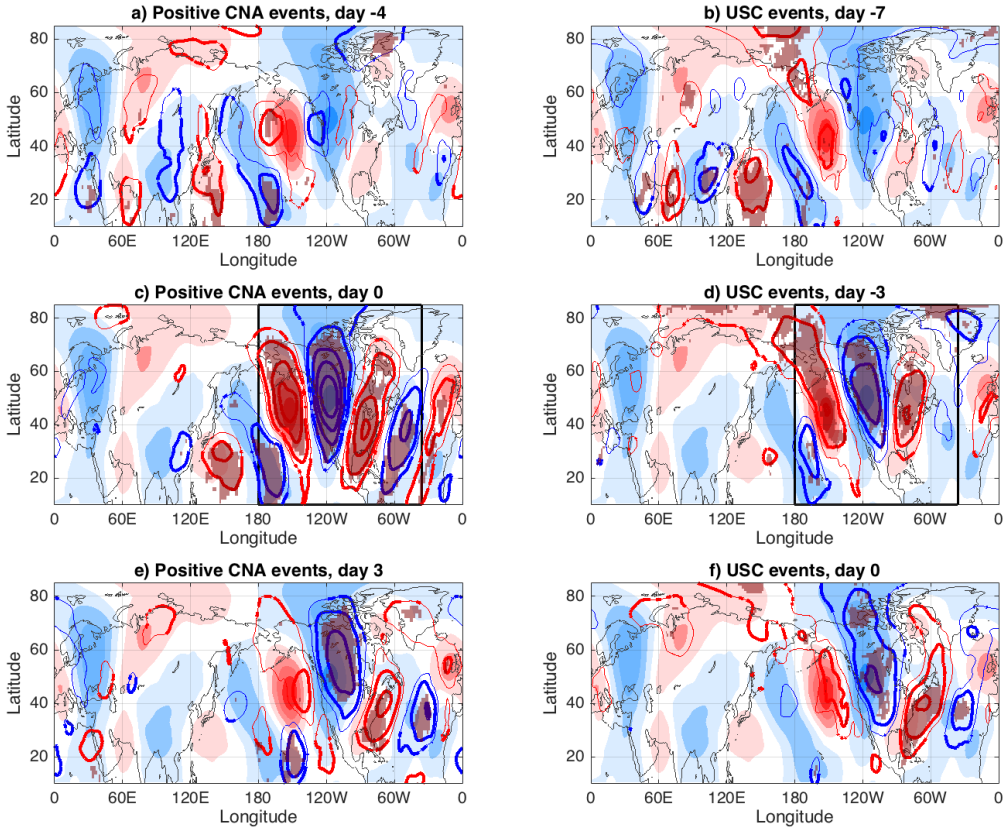

Figure 2. Time lagged composite of $300 - hPa$ meridional wind anomalies (contours) for a,c,d) positive CNA events at lags -4, 0 and 3 days; b,d,f) USC events at lags -7, -3 and 0; all plotted over the $300 - hPa$ meridional wind anomalies corresponding to the second CTP pattern (shading). The projection region used to define the CNA events is marked by the black rectangle in panels c,d. Contour interval is $5m/sec$, with the $\pm 2.5m/sec$ contours added. For contours and shading, red is positive, blue is negative. Thick contours mark 95% statistical significance, green shading marks regions where 67% of the composite members have the same sign of the composite (chances of this happening randomly are well below the 5%).

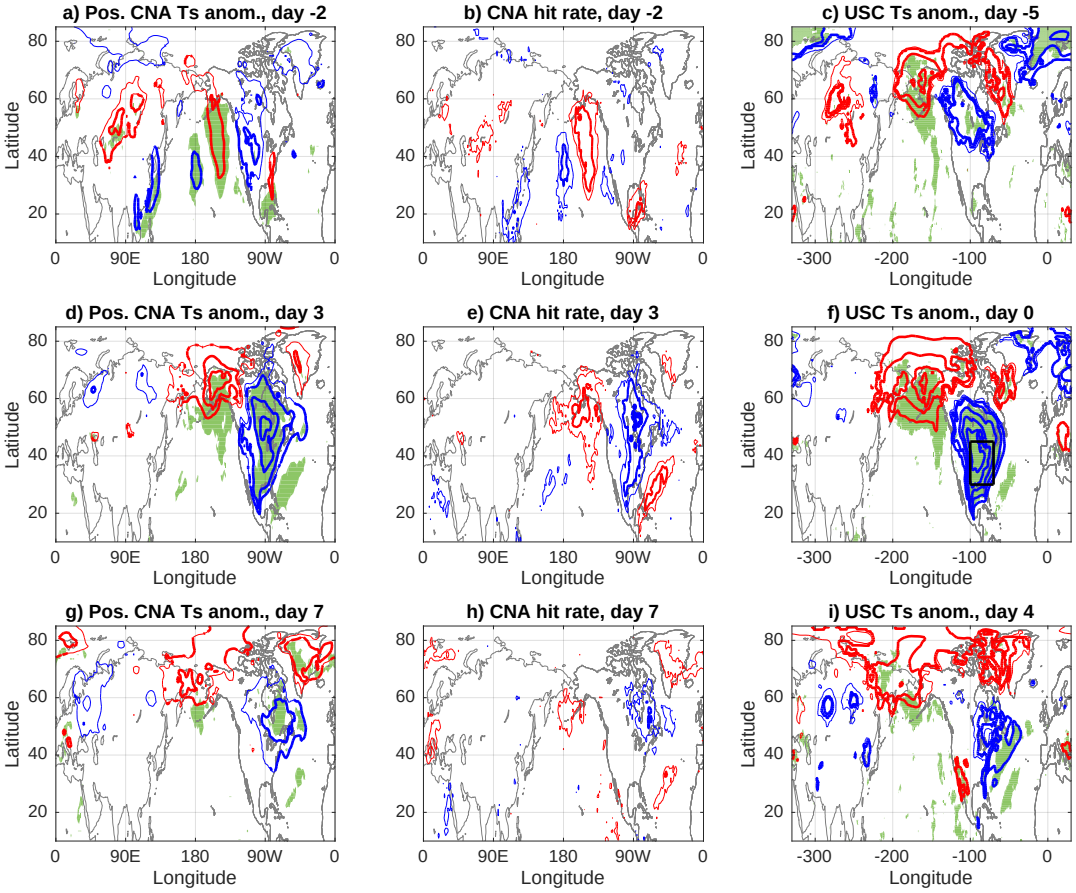

Figure 3. a,d,g) Time lagged composite of surface temperature anomalies (contours, red positive blue negative) for positive CNA events at lags -2, 3 and 7 days. Contour interval is $2K$ with the $\pm 1K$ contours added. Thick contours mark values statistically significant at the 95% level, darker shadings mark regions where 67% of the composite members have the same sign of the composite itself (chances of this happening randomly are well below 5%). b,e,h) The percent of positive CNA composite members (in a,d,g respectively) which have the same sign as the composite. Contours mark 65%, 75%, and 85% (marked by increasing thickness), with red/blue marking regions where the composite mean is positive/negative. c,f,i) same as a,d,g but for USC events but at lags -5, 0 and 4 days; The black rectangle in panel f shows the region used to define the USC events.

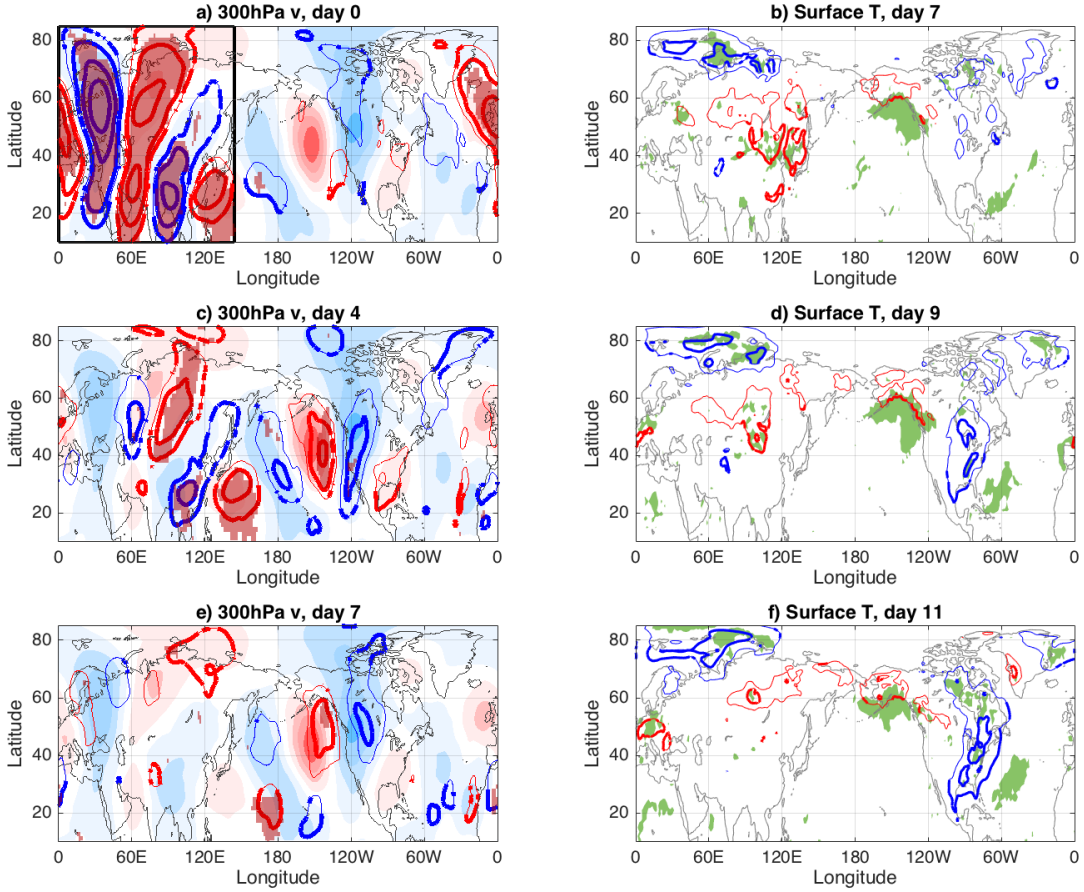

Figure 4. Precursor wave packet time lagged composites of: a,c,e) $300 - hPa$ meridional wind anomalies at days 0, 4, 7 (contours, interval $5m/sec$ with the $\pm 2.5m/sec$ contours added); b,d,f) surface temperature anomalies at lags 7, 9, and 11 days (contours, interval $2m/sec$ with the $\pm 1m/sec$ contours added). The composites are for events when the $300 - hPa$ meridional wind projects maximally onto the Euro-Asian sector (marked by the black rectangle in panel a), using 79 events. Also shown in panels (a,c,e) are the $300 - hPa$ meridional wind anomalies corresponding to the second CTP pattern. For contours and shadings, red is positive and blue is negative. Thick contours mark values statistically significant at the 95% level, and the darker shading on a,c,e and green shading on b,d,f mark regions where 67% of the composite members have the same sign of the composite itself (chances of this happening randomly are well below 5%).

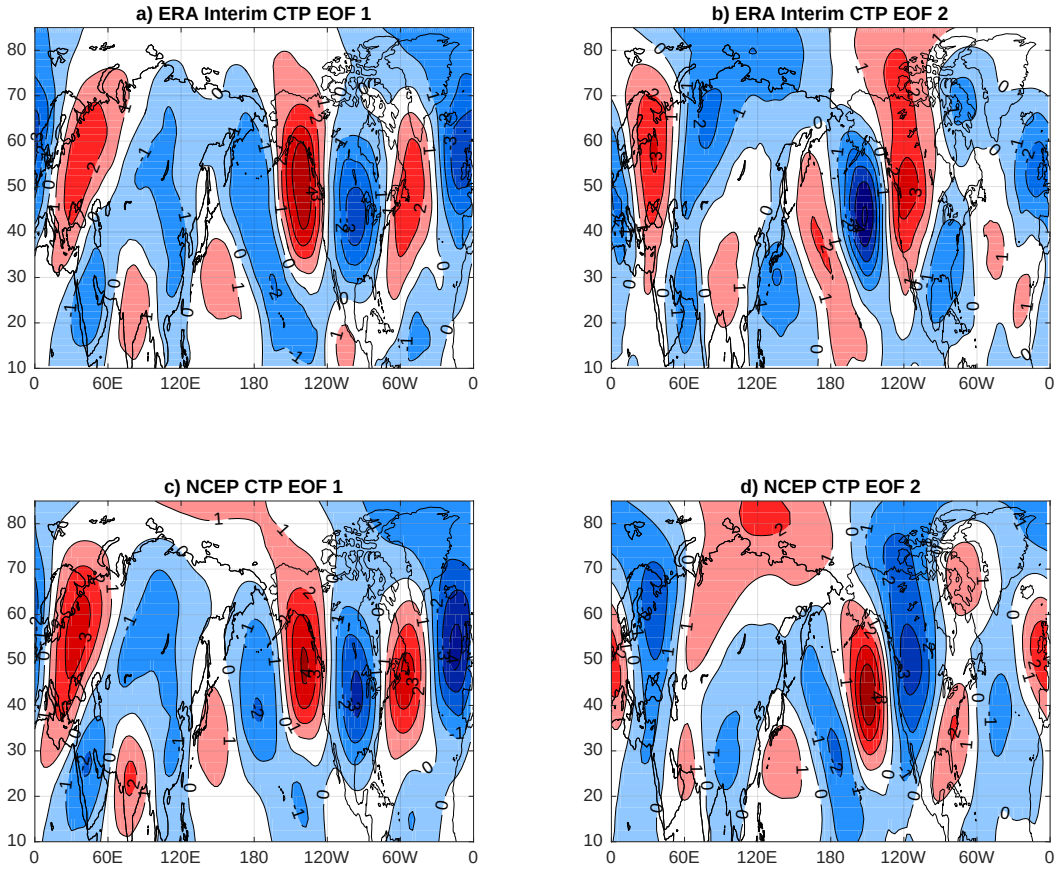

391 **Figure S1.** The first two CTP EOF patterns using ERA-Interim (top row) and NCEP (bottom row). EOF 1
392 (left) and EOF 2 (right) in ERA-Interim explain $13.3 \pm 1.8\%$ and $11.5 \pm 1.6\%$ of the variance. These EOFs
393 in NCEP explain $13.6 \pm 1.5\%$ and $10.8 \pm 1.2\%$ of the variance

.

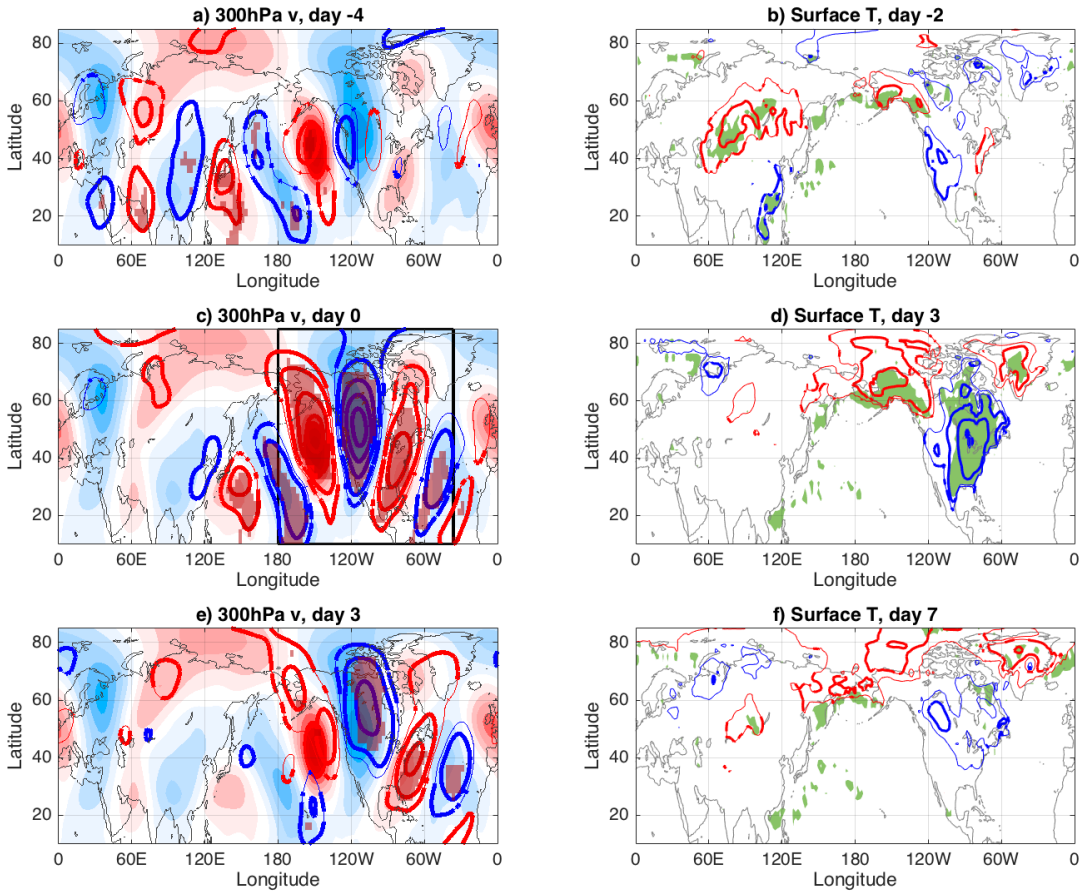

394 **Figure S2.** As in the left columns of figures 2 and 3 but using NCEP data. Note the absence of the
395 ocean surface air temperature anomalies found for ERA-Interim (Figure 2a,c,e), despite the similarities of
396 $300 - hPa$ v between the two data sets (compare to Figure 3a,c,e). Since there are 123 events for this data
397 set, the chances to randomly get 67% of the composite members with the same sign of the composite itself are
398 0.03%.

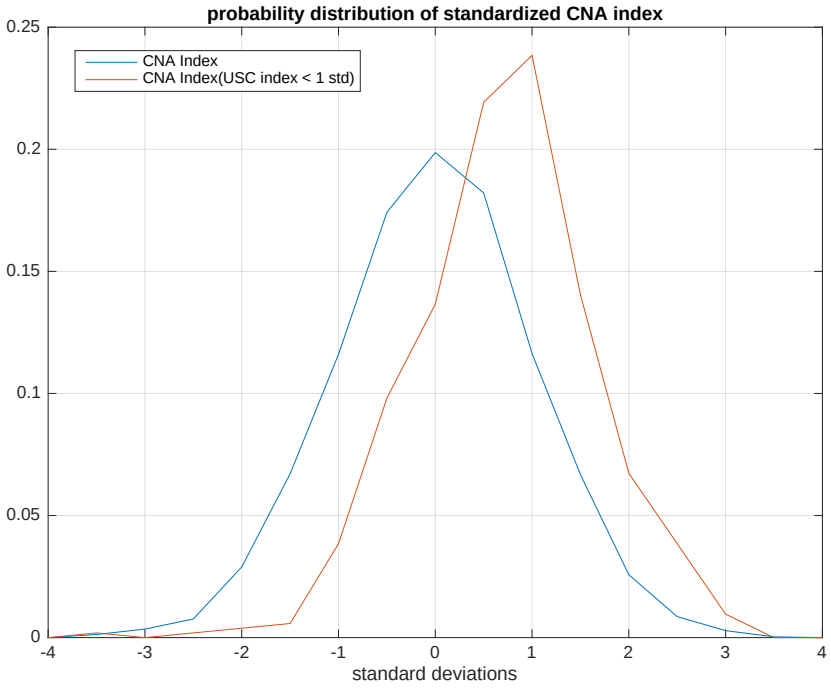

Figure S3. The probability distribution function (pdf) of the Dec-Feb standardised CNA index values for all days (blue) and for days which are followed 3 days later by a USC index below -1 standard deviations (red).

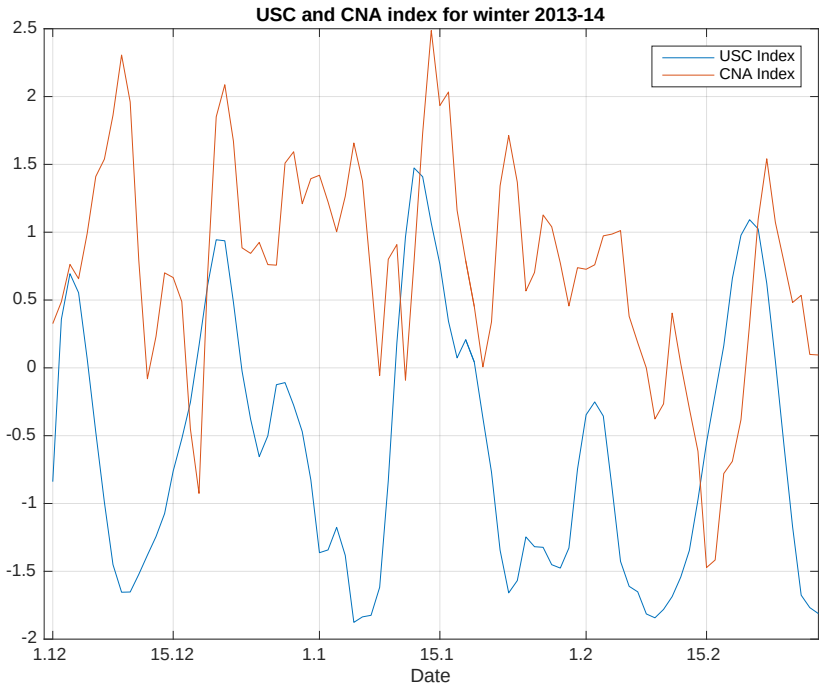

Figure S4. The daily CNA (red) and USC (blue) standardised index time series for the winter of 2013-14 (1 Dec 2013 - 28 Feb 2014). We subtracted the mean Dec-Feb value between Dec 1st 1979 and Feb 28th 2014, and divided by the standard deviation.

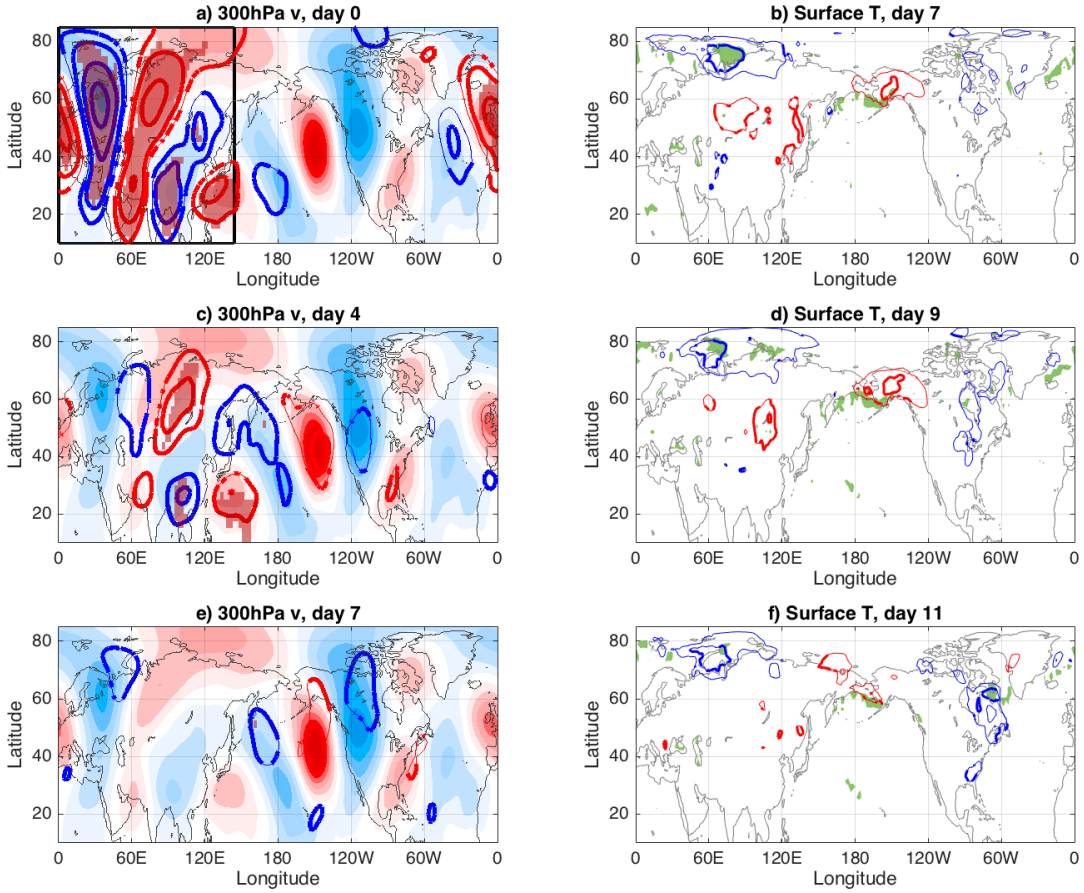

Figure S5. As in figure 4 but using NCEP data. Note again the absence of the ocean surface air temperature anomalies found for ERA-Interim and the smaller eastern North America 2-meter temperature anomaly at lag 11 days. The composites are based on 139 events, and the chances to randomly get 67% of the composite members with the same sign of the composite itself are less than 0.01%.